How Much Oxygen Can a MXene Surface Take Before It Breaks?

Persson, Ingemar; Halim, Joseph; Hansen, Thomas Willum; Wagner, Jakob Birkedal; Darakchieva, Vanya; Palisaitis, Justinas; Rosen, Johanna; Persson, Per O. Å.

Published in:
Advanced Functional Materials

Link to article, DOI:
10.1002/adfm.201909005

Publication date:
2020

Document Version
Publisher's PDF, also known as Version of record

ADVANCED FUNCTIONAL MATERIALS
www.afm-journal.de

How Much Oxygen Can a MXene Surface Take Before It Breaks?

*Ingemar Persson, Joseph Halim, Thomas W. Hansen, Jakob B. Wagner, Vanya Darakchieva, Justinas Palisaitis, Johanna Rosen, and Per O. Å. Persson**

Tuning and tailoring of surface terminating functional species hold the key to unlock unprecedented properties for a wide range of applications of the largest 2D family known as MXenes. However, a few routes for surface tailoring are explored and little is known about the extent to which the terminating species can saturate the MXene surfaces. Among available terminations, atomic oxygen is of interest for electrochemical energy storage, hydrogen evolution reaction, photocatalysis, etc. However, controlled oxidation of the surfaces is not trivial due to the favored formation of oxides. In the present contribution, single sheets of $Ti_3C_2T_x$ MXene, inherently terminated by F and O, are defluorinated by heating in vacuum and subsequentially exposed to O_2 gas at temperatures up to 450 °C in situ, in an environmental transmission electron microscope. Results include exclusive termination by O on the MXene surfaces and eventual supersaturation ($x > 2$) with a retained MXene sheet structure. Upon extended O exposure, the MXene structure transforms into TiO_2 and desorbs surface bound H_2O and CO_2 reaction products. These results are fundamental for understanding the oxidation, the presence of water on MXene surfaces, and the degradation of MXenes, and pave way for further tailoring of MXene surfaces.

1. Introduction

Research in 2-dimensional (2D) materials has expanded tremendously over the last decade, motivated by outstanding properties and a broad spectrum of applications.[1] Electrochemical energy storage and catalysis, such as supercapacitors[2] and hydrogen evolution reaction (HER),[3,4] to mention a few, greatly benefits from the immense active surface that can be realized by 2D materials.[5–7] MXenes constitute the largest and continuously growing family of 2D materials.[8,9] From applications in, energy storage,[2] to cationic adsorption,[10] electromagnetic interference shielding,[11] and carbon capture,[12] MXenes have emerged with superior properties and performance. MXenes are obtained from the atomically laminated parent MAX phases, typically described by the formula $M_{n+1}AX_n$ ($n = 1–3$).[13] The MAX structure consists of transition metal layers (M) that interleave C and/or N layers (X). The strongly bonded MX slabs are further separated by an atomically thin layer of a group 13 or 14 element (A).[8] MXenes are typically produced from MAX phases by chemical etching of the weakly bonded A layers. During etching, the highly reactive transition metal surfaces are instantly terminated by species from the etchant, T_x,[14,15] resulting in the general MXene formula $M_{n+1}X_nT_x$. The MXenes are highly versatile and allow for property tuning through variations in structure, composition and surface terminations. The MXene structure is primarily given by the number of M and X layers (n), while the compositional tuning (more than 30 MXenes have been realized) on the other hand offer a vast space of tuning opportunity. Varying M and/or X elements[11,12] or alloying on either or both M and X[9,16] has previously been demonstrated. Furthermore, MXenes can be realized with two M elements ordered out-of-plane,[17] in-plane,[18] and finally with vacancy ordered[19,20] structures. In addition, MXene synthesis is potentially scalable, which renders the MXenes unique in the 2D materials community.[21]

The remaining route for property tuning, through manipulation of the surface terminations, has received far less attention, as they are native to the etchant and it has been difficult to control their composition. T_x is generally considered to be a combination of O, OH, and F,[22,23] and their influence

Dr. I. Persson, Dr. J. Halim, Dr. J. Palisaitis, Prof. J. Rosen, Prof. P. O. Å. Persson
Thin Film Physics Division
Department of Physics
Chemistry and Biology (IFM)
Linköping University
SE-581 83 Linköping, Sweden
E-mail: per.persson@liu.se
Dr. T. W. Hansen, Prof. J. B. Wagner
Center for Electron Nanoscopy
DTU Danchip/CEN
DK-2800, Kgs. Lyngby, Denmark
Dr. V. Darakchieva
Center for III-Nitride Technology
C3NiT-Janzén and Terahertz Materials Analysis Center
Department of Physics Chemistry and Biology (IFM)
Linköping University
SE-581 83 Linköping, Sweden
The ORCID identification number(s) for the author(s) of this article can be found under https://doi.org/10.1002/adfm.201909005.

DOI: 10.1002/adfm.201909005

on MXene properties has been theoretically investigated.[24] Recently, Cl was added to the list of terminations and was demonstrated as an exclusive termination.[25] Previous efforts have shown that it is possible to vary the amount of F and O through the etchant,[16] while keeping the overall number of terminations constant. Exclusive termination by O ($M_{n+1}X_nO_2$) was predicted by theoretical means to improve the volumetric capacity of supercapacitors,[26,27] and the catalytic efficiency in HER applications.[3,4] Furthermore, fully O-terminated $Ti_3C_2T_x$ has also been considered as a promising NH_3 selective adsorber.[28]

Consequently, attempts to fully terminate $Ti_3C_2T_x$ MXene by O has been performed, however, with reports on the formation of oxides[29–31] and property degradation through a structural transformation of the MXene sheet. Therefore, the oxidation behavior and the degradation mechanism of MXenes constitute essential knowledge in the MXene field.

Herein, we apply an initial defluorination process to remove the native F terminations while keeping the native O terminations.[22] Subsequentially, the MXene surfaces are exposed to a controlled O_2 environment, which results in the exclusive termination by O. With increasing exposure and temperature, the MXene surfaces are supersaturated ($x > 2$) which is highly significant as this has not been shown before and because an increased number of O on the surface was predicted to directly increase the number of active sites for H^+ evolution.[4] Upon extended exposure the MXene structure eventually breaks down, which results in the desorption of H_2O and the formation of 2D amorphous Ti(C, O)$_2$ and TiO_2 nanoparticles.

2. Results and Discussion

Single $Ti_3C_2T_x$ flakes, inherently terminated by F and O, were subjected to an initial high-temperature treatment to remove the F-terminations and leaving parts of the MXene surface nonterminated, see Figure S1 in the Supporting Information.[22] The O-saturation process was followed in situ by high-resolution TEM (HRTEM) imaging, electron energy-loss spectroscopy (EELS), and electron diffraction (ED) in high vacuum after sequential 2 mbar O_2 exposures from room temperature (RT) and up to 450 °C. The reaction products were monitored by simultaneous residual gas analysis (RGA).

Figure 1 presents plan-view HRTEM images acquired from 1 to 3 superimposed $Ti_3C_2O_x$ single sheets after O_2 exposures at a) RT, b) 100 °C, c) 175 °C, d) 350 °C, e) 400 °C, and f) 450 °C. The sites, from which the images originate, differ to avoid unintentional electron beam induced artefacts to the MXene sheet. A gradual increase in disorder (in terms of the total area of features obscuring the MXene lattice) is observed from RT to 400 °C, which is also visible through the fast Fourier transform (FFT) insets, where a diffuse centrosymmetric background represent disorder (for the employed Gaussian defocus), e.g., at 400 °C, the MXene lattice is barely visible in the image, but a periodicity is registered through the FFT. The large field-of-view HRTEM images from which the FFTs are obtained, can be found in Figure S2 in the Supporting Information. At 450 °C, the MXene structure has disappeared; however, it should be noted that the 2D nature of the sheet is preserved, in line with a previous report on high-temperature oxidation,[30–32] see Figure S3 in the Supporting Information.

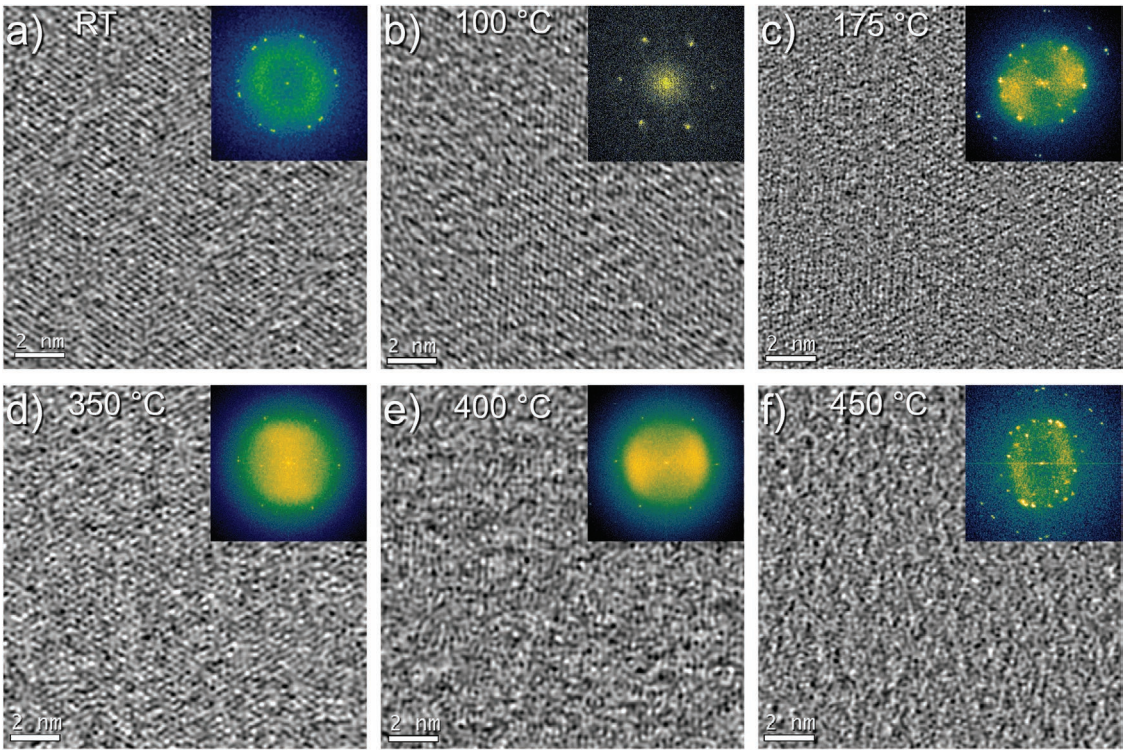

Figure 1. Plan-view HRTEM images acquired from 1 to 3 $Ti_3C_2T_x$ stacked single flakes after exposure to 2 mbar O_2 gas for 0.5 h, at a) RT, b) 100 °C, c) 175 °C, d) 350 °C, e) 400 °C, and f) 450 °C. Insets show corresponding FFTs from a larger field of view (70 nm × 70 nm).

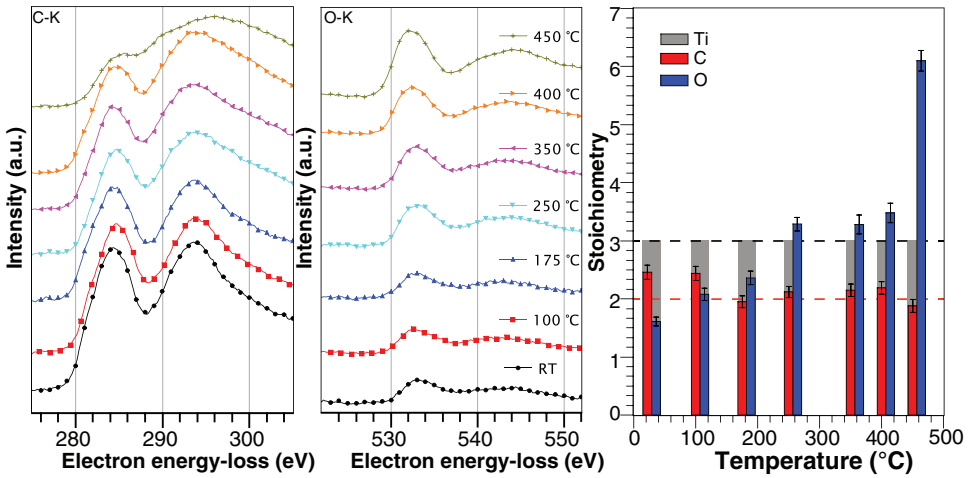

Figure 2. EELS spectra of C-K and O-K edges acquired from $Ti_3C_2T_x$ flakes after exposure to 2 mbar O_2 gas for 0.5 h, at RT, 100 °C, 150 °C, 175 °C, 250 °C, 350 °C, 400 °C, and 450 °C. C/Ti/O stoichiometries as obtained by EELS quantification from RT to 450 °C. All spectra are normalized against the Ti-L edge (Figure S4, Supporting Information) that was presumed stationary throughout the heating and gas exposure experiments. Dashed lines indicate the expected ratio of Ti and C in $Ti_3C_2T_x$.

Figure 2 shows the EELS spectra of C-K and O-K edges, after background-subtraction and plural-scattering deconvolution, from RT to 450 °C. The corresponding edge intensities are normalized versus the Ti edge (Figure S4, Supporting Information), since the number of Ti atoms are presumed to remain constant (Ti is not sputtered or desorbed). The sheet stoichiometries were obtained by EELS quantification of the C-K, Ti-$L_{2,3}$, and O-K edges at corresponding temperatures. It should be noted that the changes in the composition were reached fairly instantly (matter of seconds), while the exposures were extended for 30 min to accommodate for the response time of the RGA for each temperature interval.

Following the initial high-temperature defluorination the relative stoichiometry showed a slightly higher C content than expected for $Ti_3C_2T_x$. This is attributed to ambient temperature hydrocarbon adsorption on the vacated F-sites due to the highly reactive nature of the bare MXene surface and the vacuum conditions of the microscope. However, the relative C content, hence the adsorbed hydrocarbons, is observed to decrease (hydrocarbon desorption) during exposures and heating from RT to 175 °C. At this point the stoichiometry approaches the anticipated proportions for Ti_3C_2 MXene. From thereon, the C stoichiometry remains stable until the final exposure at 450 °C after which an ≈14% decrease of C (relative Ti) is observed. The O content at the onset of the experiment, after defluorination, corresponds to a coverage of 0.8 O atoms per surface Ti atom ($x = 1.6$). The surface is saturated by O at 100 °C ($x = 2$) and the oxygen content is relatively stable until a temperature of 250 °C is reached when a sudden increase is observed ($x > 3$) which implies a supersaturated surface with 1.5 adsorbed O atoms per surface Ti atom. The composition remains relatively stable from there on, with a minor increase observed at 400 °C, reaching a coverage corresponding to 1.74 O atoms ($x = 3.48$) per surface Ti atom. At 450 °C, a significant change in the EELS spectrum is observed, which corresponds to the reduction in the C content and with the Ti:O content approaching that of TiO_2.

A closer inspection of the EELS spectra reveals that the C-K edge is unchanged until 450 °C at which point the onset peak (284 eV) is diminished, shifted +0.4 eV and experiences a fine structure change, where part of its intensity is shifted toward a shoulder centered at ≈290 eV, indicating carboxide (C_yO_z) formation.[33] Furthermore, the Ti-L_3 (Figure S4, Supporting Information) peak is shifted +0.5 eV while Ti-L_2 is shifted +0.2 eV. In contrast, the O-K edge experiences an energy shift of −1 eV. These combined energy shifts of C-K, Ti-$L_{2,3}$, and O-K at 450 °C together with the observed increase in O content indicate a charge transfer from Ti and C to O, attributed to the higher electronegativity of O as a consequence of the formation of additional Ti—O, new C—O bonds, and a reduction of Ti—C bonds. It should also be noted that an increase in O signal due to intercalation of molecular O_2 between sheets is ruled out, by the absence of the specific chemical signature of O_2 compared to MXene bonded O, see Figure S5 in the Supporting Information.

Figure 3 presents ED patterns at RT, 175, 350, and 450 °C. The diffraction spots corresponding to $Ti_3C_2T_x$ 110 (1.543 Å) and 100 (2.672 Å) reciprocal lattice points are dominant after O exposure from RT to 400 °C. This evidences that the MXene structure remains intact until 400 °C in agreement with TEM results displayed in Figure 1. However, at 450 °C a new set of reflections appears, while the 110 and 100 $Ti_3C_2T_x$ reflections are significantly reduced in intensity. A detailed inspection shows that these reflections exhibits lattice spacings that corresponds to TiO_2 rutile, brookite and/or anatase nanoparticle formation (see Figure S6 and Table S1 in the Supporting Information), in line with previous reports.[31,34] In contrast to the ED patterns for lower temperatures, the ED pattern at 450 °C exhibit a diffuse centrosymmetric background that indicates amorphization of the sheet.

Figure 4a displays the RGA spectra for the mass numbers; 32, 18, and 44, corresponding to O_2, H_2O, and CO_2 acquired in operando. The plateau/valley features in the RGA data corresponds to the iterative O_2 exposure (plateau) and evacuation (valley) procedure prior to imaging and spectroscopy. The temperature is indicated for each cycle in the figure. A continuous decrease of H_2O is observed from RT until 400 °C, attributed to background desorption of the sample. However, at 450 °C

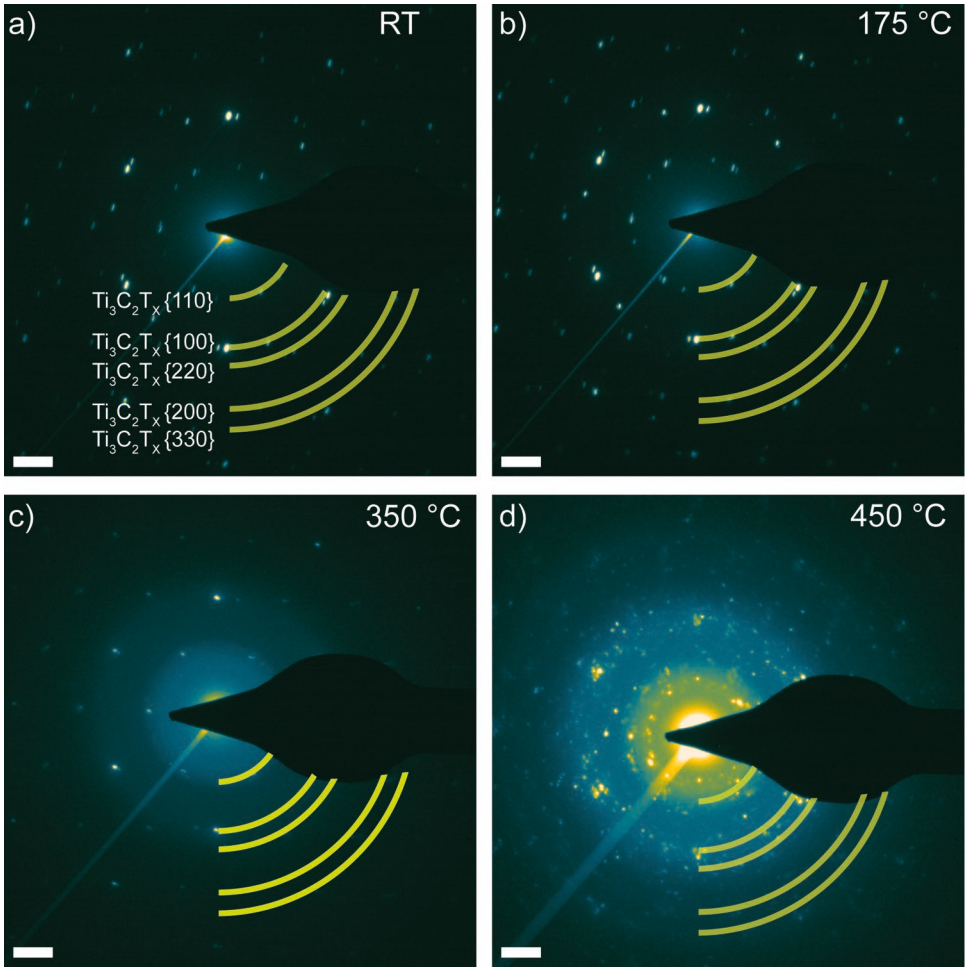

Figure 3. ED patterns acquired from $Ti_3C_2T_x$ flakes in vacuum after exposure to 2 mbar O_2 gas for 0.5 h, at a) RT, b) 175 °C, c) 350 °C, and d) 450 °C. Scale bars indicate 2 (1/nm).

(Figure 4a,b) an apparent increase in H_2O is detected. As the volume that is heated by the microheater is very small, it is improbable that the sudden change in residual H_2O is caused by background degassing, particularly after the initial defluorination at 700 °C followed by the continuously reducing RGA background after O_2 exposures. A similar increase at 450 °C is noted for CO_2, however, an order of magnitude lower than the H_2O (see Figure 4a,b). Additionally, masses corresponding to N, CH, CH_3, and H_2 were monitored. In contrast to H_2O and CO_2 no increase was observed for these gasses during the high-temperature O_2 exposures.

The MXene structure is preserved after O_2 exposure up to 400 °C as evidenced by ED and RGA as no phase transformation occurs and no reaction products are detected. However, the TEM images shows an increased disorder which is correlated to an increased O content as evidenced by EELS. The observed disorder can be understood by the increasing O supersaturation ($x > 2$) of the MXene surface, where initially, the O atoms occupy the preferred site (fcc), while upon saturation, the O atoms occupy less favored but energetically comparable alternative sites.[22,35] The O supersaturation is further proposed to cause disorder among the surface Ti layer atoms, which explains the increasing disorder observed in the TEM images. The corresponding situation was, however, investigated from a theoretical viewpoint and showed that supersaturation of O on MXene surfaces was favored in high-temperature oxidizing environments (albeit at very high temperatures but at shorter time scales).[30] The report also suggests that a structural transformation into carbon supported titania is finally achieved by Ti diffusion to the sheet surface. The observed supersaturation is however in contrast to most experimental and theoretical viewpoints on MXenes, that the available termination sites limit $x \leq 2$ in $Ti_3C_2T_x$.

The present results show that oxygen binds to the MXene surface, when energy is supplied to the surface (through heating) that lead to increasing supersaturation and final breakdown of the structural integrity at 450 °C. Following this result, an intrinsically less stable structure such as Ti_2C[36] that does not exhibit a stabilizing core M layer would presumably degrade at even lower temperatures during oxygen exposure.

At 450 °C, the formation of TiO_2 nanoparticles and amorphization of $Ti_3C_2T_x$ is confirmed by ED. Moreover, EELS evidences carboxides and TiO_2 formation that most likely is the dominant contribution to the amorphous signal observed by ED. Upon the transformation into TiO_2, an ≈14% decrease in the C-K signal is noted, which is attributed to the detected

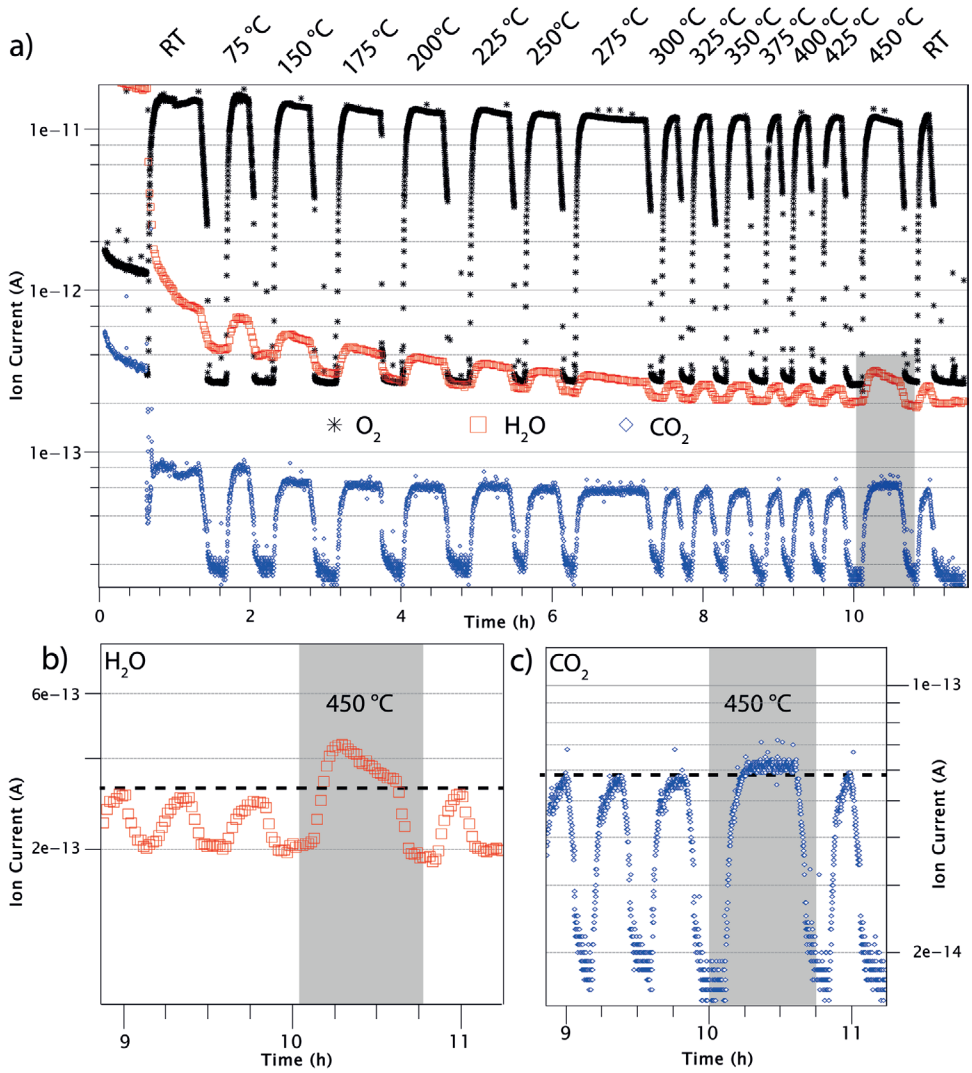

Figure 4. a) RGA spectra of O_2, H_2O, and CO_2 acquired during 2 mbar O_2 exposure from RT to 450 °C. The O_2 was pumped out prior to imaging and EELS acquisition leading to the plateaus/valleys in the spectra. The insets reveal an enlarged view of the b) H_2O and c) CO_2, specifically in temperature window of 450 °C (indicated by the shaded area). The dashed lines identify the max current prior to the 450 °C cycle.

CO_2 desorption (RGA). Put together, the extended oxidation of $Ti_3C_2T_x$ at increasing temperature suggests the following irreversible reaction path for the MXene transformation into titania

$$Ti_3C_2O_2 + 4O_2 \rightarrow 3TiO_2 + 2CO_2 \quad (1)$$

This reaction, on the other hand, does not explain the desorption of water. Presumably, the detected water was originally chemisorbed on the MXene surface, as recently shown theoretically,[37] and then immediately desorbed during the MXene transformation into titania since, water is known to desorb from titania at much lower temperatures.[38] The identification of chemisorbed water on the MXene surface has not been considered until presently. MXenes are prone to intercalate and physisorb H_2O; however, physisorbed water is weakly bonded and desorb after heating above 200 °C.[39] Herein, the H_2O remains present even after preheating at 700 °C in vacuum.

The results presented here is of immediate and fundamental consequence to the MXene field. Foremost, we demonstrate exclusive O-saturation of Ti_3C_2 surfaces by a facile postprocessing route. In addition, although attempts have been made to increase the O content on MXene surfaces,[30,31] this is the first experimental investigation to verify supersaturation of O on the MXene surface, that is not associated with a structural transformation into carbon supported titania, owing to the initial deflourination process.

3. Conclusions

In the present investigation, we have presented a route toward exclusive termination of $Ti_3C_2T_x$ MXene surfaces by O, which is of fundamental importance for advanced applications such as in electrochemical energy storage and catalytic processes. We have additionally shown that the O terminations can reach

supersaturation with $x \approx 3.5$ while maintaining the structural integrity of the MXene sheet. This is additionally of fundamental consequence for MXenes as the saturation is widely considered to be one terminating species per surface transition metal element. A higher O coverage in combination with higher processing temperatures results in amorphization of the sheet and/ or formation of TiO_2 phases though the 2D nature of the flake persists. Finally, with extended oxidation at 450 °C, the MXene sheet was structurally transformed into crystalline titania and amorphous $Ti(C,O)_2$. While the MXene transforms into titania, H_2O and CO_2 are desorbed. CO_2 is a product of the titania transformation and H_2O is proposed to originate from chemisorbed water on the MXene surface that is released because of the lower H_2O desorption temperature of titania compared to MXenes. This is perhaps the most fundamental observation of this investigation as water has hitherto not been considered as a terminating specie.

4. Experimental Section

$Ti_3C_2T_x$ singe-flake colloidal suspension was prepared by LiF and HCl etching of Ti_3AlC_2 and delaminated into 20 × 20 µm large flakes by shaking in deionized water according to steps previously described.[15] TEM samples were thereafter prepared by drop-casting 0.1 µL single-flake dispersion on a DENSsolutions through-hole Wildfire nanoreactor chip and placed in a DENSsolutions single-tilt heating holder. The image corrected FEI Titan environmental transmission electron microscope (ETEM) at DTU equipped with a high brightness XFEG and a monochromator operated at 300 kV with 0.8 Å resolution was used to characterize the surface of single flakes before, during and after O_2 gas exposure at various temperatures. EELS was acquired using a GIF Tridiem at 1.3 eV energy resolution in diffraction mode with an ≈0 mrad convergence angle and an ≈10 mrad collection angle. Spectra were acquired after 1, 5, 10, 20, and 30 min exposure times of 2 mbar O_2 in order to rule out time dependency. The intensity of all spectra was normalized against Ti-$L_{2,3}$. RGA data were acquired with a Pfeiffer Vacuum analyzer. HRTEM images were acquired with the Gatan OneView 4K CMOS camera. EELS data processing was performed using the commercial Gatan Digital Micrograph software with built in routines. Quantification was done on single-scattering distributions after Fourier deconvolution and employing Hartree–Slater inelastic electron scattering cross-section, excluding energy-loss near edge structures.

Supporting Information

Supporting Information is available from the Wiley Online Library or from the author.

Acknowledgements

The authors acknowledge the Swedish Research Council for funding under Grant Nos. 2016-04412, 2016-00889 and 642-2013-8020, the Knut and Alice Wallenberg's Foundation for support of the electron microscopy laboratory in Linköping, a fellowship grant and a project grant (KAW 2015.0043). The authors also acknowledge Swedish Foundation for Strategic Research (SSF) through the Research Infrastructure Fellow program no. RIF 14-0074 and the Future Research Leaders Grant FL12-0181. The authors finally acknowledge support from the Swedish Government Strategic Research Area in Materials Science on Functional Materials at Linköping University (Faculty Grant SFO-Mat-LiU No. 2009 00971).

Conflict of Interest

The authors declare no conflict of interest.

Author Contributions

P.O.Å.P. conceived the research plan with input from I.P. and J.R. The materials were prepared by J.H. I.P. performed the experimental work and the analysis under supervision of T.W.H., J.B.W., and P.O.Å.P. The manuscript was drafted by I.P. and finalized with input from all authors.

Keywords

2D materials, environmental TEM, MXene, surface terminations

Received: October 30, 2019
Revised: January 8, 2020
Published online:

[1] S. Z. Butler, S. M. Hollen, L. Cao, Y. Cui, J. A. Gupta, H. R. Gutiérrez, T. F. Heinz, S. S. Hong, J. Huang, A. F. Ismach, E. Johnston-Halperin, M. Kuno, V. V. Plashnitsa, R. D. Robinson, R. S. Ruoff, S. Salahuddin, J. Shan, L. Shi, M. G. Spencer, M. Terrones, W. Windl, J. E. Goldberger, *J. Am. Chem. Soc.* **2013**, *7*, 2898.
[2] B. Anasori, M. R. Lukatskaya, Y. Gogotsi, *Nat. Rev. Mater.* **2017**, *2*, 16098.
[3] C. Ling, L. Shi, Y. Ouyang, J. Wang, *Chem. Mater.* **2016**, *28*, 9026.
[4] G. Gao, A. P. O'Mullane, A. Du, *ACS Catal.* **2017**, *7*, 494.
[5] H. Zhang, X. Lv, Y. Li, Y. Wang, J. Li, *ACS Nano* **2010**, *4*, 380.
[6] J. Low, L. Zhang, T. Tong, B. Shen, J. Yu, *J. Catal.* **2018**, *361*, 255.
[7] J. Ran, G. Gao, F.-T. Li, T.-Y. Ma, A. Du, S.-Z. Qiao, *Nat. Commun.* **2017**, *8*, 13907.
[8] M. Naguib, M. Kurtoglu, V. Presser, J. Lu, J. J. Niu, M. Heon, L. Hultman, Y. Gogotsi, M. W. Barsoum, *Adv. Mater.* **2011**, *23*, 4248.
[9] M. Naguib, O. Mashtalir, J. Carle, V. Presser, J. Lu, L. Hultman, Y. Gogotsi, M. W. Barsoum, *ACS Nano* **2012**, *6*, 1322.
[10] Q. Peng, J. Guo, Q. Zhang, J. Xiang, B. Liu, A. Zhou, R. Liu, Y. Tian, *J. Am. Chem. Soc.* **2014**, *136*, 4113.
[11] F. Shahzad, M. Alhabeb, C. B. Hatter, B. Anasori, S. Man Hong, C. M. Koo, Y. Gogotsi, *Science* **2016**, *353*, 1137.
[12] I. Persson, J. Halim, H. Lind, T. W. Hansen, J. B. Wagner, L.-Å. Näslund, V. Darakchieva, J. Palisaitis, J. Rosen, P. O. Å. Persson, *Adv. Mater.* **2019**, *31*, 1805472.
[13] M. W. Barsoum, *Prog. Solid State Chem.* **2000**, *28*, 201.
[14] M. Naguib, V. N. Mochalin, M. W. Barsoum, Y. Gogotsi, *Adv. Mater.* **2014**, *26*, 992.
[15] P. Srivastava, A. Mishra, H. Mizuseki, K.-R. Lee, A.K. Singh, *ACS Appl. Mater. Interfaces* **2016**, *8*, 24256.
[16] M. Naguib, J. Halim, J. Lu, L. Hultman, Y. Gogotsi, M. W. Barsoum, *J. Am. Chem. Soc.* **2013**, *135*, 15966.
[17] B. Anasori, Y. Xie, M. Beidaghi, J. Lu, B.C. Hosler, L. Hultman, P. R. C. Kent, Y. Gogotsi, M. W. Barsoum, *ACS Nano* **2015**, *9*, 9507.
[18] I. Persson, A. el Ghazaly, Q. Tao, J. Halim, S. Kota, V. Darakchieva, J. Palisaitis, M. W. Barsoum, J. Rosen, P. O. Å. Persson, *Small* **2018**, *14*, 1703676.
[19] Q. Tao, M. Dahlqvist, J. Lu, S. Kota, R. Meshkian, J. Halim, J. Palisaitis, L. Hultman, M. W. Barsoum, P. O. Å. Persson, J. Rosen, *Nat. Commun.* **2017**, *8*, 14949.

[20] R. Meshkian, M. Dahlqvist, J. Lu, B. Wickman, J. Halim, J. Thörnberg, Q. Tao, S. Li, S. Intikhab, J. Snyder, M. W. Barsoum, M. Yildizhan, J. Palisaitis, L. Hultman, P. O. Å. Persson, J. Rosen, *Adv. Mater.* **2018**, *30*, 1706409.
[21] M. Alhabeb, K. Maleski, B. Anasori, P. Lelyukh, L. Clark, S. Sin, Y. Gogotsi, *Chem. Mater.* **2017**, *29*, 7633.
[22] I. Persson, L.-Å. Näslund, J. Halim1, M. W. Barsoum, V. Darakchieva, J. Palisaitis, J. Rosen, P. O. Å. Persson, *2D Mater.* **2018**, *5*, 015002.
[23] M. A. Hope, Al. C. Forse, K. J. Griffith, M. R. Lukatskay, M. Ghidiu, Y. Gogotsi, C. P. Grey, *Phys. Chem. Chem. Phys.* **2016**, *18*, 5099.
[24] M. Khazaei, A. Ranjbar, M. Arai, T. Sasaki, S. Yunoki, *J. Mater. Chem. C* **2017**, *5*, 2488.
[25] J. Lu, I. Persson, H. Lind, M. Li, Y. Li, K. Chen, J. Zhou, S. Du, Z. Chai, Z. Huang, L. Hultman, J. Rosen, P. Eklund, Q. Huang, P. O. Å. Persson, *Nanoscale Adv.* **2019**, *1*, 3680.
[26] Y. Dall'Agnese, M. R. Lukatskaya, K. M. Cook, P.-L. Taberna, Y. Gogotsi, P. Simon, *Electrochem. Commun.* **2014**, *48*, 118.
[27] Y. Xie, M. Naguib, V. N. Mochalin, M. W. Barsoum, Y. Gogotsi, X. Yu, K.-W. Nam, X.-Q. Yang, A. I. Kolesnikov, P. R. C. Kent, *J. Am. Chem. Soc.* **2014**, *136* , 6385.
[28] X.-F. Yu, Y.-C. Li, J.-B. Cheng, Z.-B. Liu, Q.-Z. Li, W.-z. Li, X. Yang, B. Xiao, *ACS Appl. Mater. Interfaces* **2015**, *7*, 13707.
[29] Y. Jiang, T. Sun, X. Xie, W. Jiang, J. Li, B. Tian, C. Su, *ChemSusChem* **2019**, *12*, 1368.
[30] R. Lotfi, M. Naguib, D. E. Yilmaz, J. Nandab, A. C. T. van Duin, *J. Mater. Chem. A* **2018**, *6*, 12733.
[31] H. Ghassemi, W. Harlow, O. Mashtalir, M. Beidaghi, M. R. Lukatskaya, Y. Gogotsi, M. L. Taheri, *J. Mater. Chem. A* **2014**, *2*, 14339.
[32] J. Palisaitis, I. Persson, J. Halim, J. Rosen, P. O. Å. Persson, *Nanoscale* **2018**, *10*, 10850.
[33] A. Tararan, A. Zobelli, A. M. Benito, W. K. Maser, O. Stéphan, *Chem. Mater.* **2016**, *28*, 3741.
[34] S. Bakardjieva, V. Stengl, L. Szatmary, J. Subrt, J. Lukac, N. Murafa, D. Niznansky, K. Cizek, J. Jirkovskyc, N. Petrovad, *J. Mater. Chem.* **2006**, *16*, 1709.
[35] T. Schultz, N. C. Frey, K. Hantanasirisakul, S. Park, S. J. May, V. B. Shenoy, Y. Gogotsi, N. Koch, *Chem. Mater.* **2019**, *31*, 6590.
[36] A. N. Enyashin, A. L. Ivanovskii, *J. Phys. Chem. C* **2013**, *117*, 13637.
[37] J. D. Gouveia, Á. Morales-García, F. Viñes, F. Illas, J. R.B. Gomes, *Appl. Catal., B* **2020**, *260*, 118191.
[38] G. B. Raupp, J. A. Dumesic, *J. Phys. Chem.* **1985**, *89*, 5240.
[39] M. Ghidiu, J. Halim, S. Kota, D. Bish, Y. Gogotsi, M. W. Barsoum, *Chem. Mater.* **2016**, *28*, 3507.